A EUROPEAN JOURNAL OF CHEMICAL BIOLOGY

CHEMBIOCHEM

SYNTHETIC BIOLOGY & BIO-NANOTECHNOLOGY

Accepted Article

Title: Photosensitised multiheme cytochromes as light-driven molecular wires and resistors

Authors: Jessica van Wonderen, Daobo Li, Samuel Piper, Cheuk Lau, Leon Piper, Christopher Hall, Thomas Clarke, Nicholas Watmough, and Julea N Butt

To be cited as: *ChemBioChem* 10.1002/cbic.201800313

Link to VoR: http://dx.doi.org/10.1002/cbic.201800313

A Journal of

ChemPubSoc Europe

WILEY-VCH

www.chembiochem.org

WILEY-VCH

FULL PAPER

Photosensitised multiheme cytochromes as light-driven molecular wires and resistors

Jessica H. van Wonderen,[a] Daobo Li,[a,b] Samuel E. H. Piper,[a] Cheuk Y. Lau, [a] Leon P. Jenner, [a] Christopher R. Hall,[a,c] Thomas A. Clarke,[a] Nicholas J. Watmough[a] and Julea N. Butt*[a]

Abstract: Multiheme cytochromes possess closely packed redox-active hemes arranged as chains spanning the tertiary structure. Here we describe five variants of a representative multiheme cytochrome engineered as biohybrid phototransducers converting light to electricity. Each variant possesses a single Cys-sulfhydryl near a terminus of the heme chain and that was efficiently labelled with a Ru(II)(bipyridine)$_3$ photosensitiser. When irradiated in the presence of a sacrificial electron donor the proteins exhibited different behaviours. Certain proteins were rapidly and fully reduced. Other proteins were rapidly semi-reduced but resisted complete photo-reduction. These findings reveal photosensitised multiheme cytochromes can be engineered to act as resistors, with intrinsic regulation of light-driven electron accumulation, and also as molecular wires with essentially unhindered photo-reduction. The observed behaviours are proposed to arise from interplay between the site of electron injection and the distribution of heme reduction potentials along the heme chain.

Introduction

Species of *Shewanella* and *Geobacter* are notable for a natural ability to exchange electrons between their internal and external environments [1]. These Gram-negative bacteria respire anaerobically by transporting electrons from the cell interior, across the cell envelope and through the extracellular matrix to reach acceptors including electrodes, Fe(III) oxide nanoparticles and other bacteria. Underpinning these electron transfer pathways are multiheme cytochromes [1-2]. Within such proteins, constellations of close packed hemes span the tertiary structures and complementary Fe(III)/(II) transitions occur at adjacent hemes. In these ways, electron exchange across and between proteins can transport electrons over distances exceeding cellular dimensions. Due to these remarkable properties multiheme cytochromes are of much interest for application in bioelectronics and bionanotechnology [3].

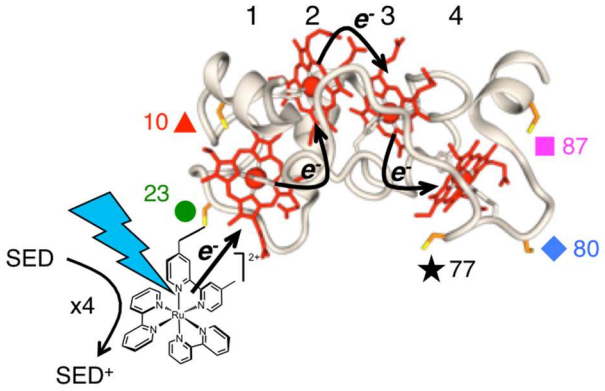

Figure 1. Ru-dye sensitised STC as phototransducer. The Ru-dye absorbs light triggering reduction of STC hemes (red) and oxidation of a molecular sacrificial electron donor (SED). Coloured symbols indicate the sites of Cys residues (carbon orange, sulfur yellow) introduced in separate proteins for attachment of the dye; STC-10 (red triangle), STC-23 (green circle), STC-77 (black star), STC-80 (blue diamond) and STC-87 (magenta square). The Ru-dye photosensitiser, RuMe, is illustrated schematically for the Λ-isomer attached at position 23. Structures were rendered with the indicated Cys introduced to STC (pdb code 1M1Q) using FoldX-YASARA [13].

The small tetraheme cytochrome STC, also known as CctA, [4] is a multiheme cytochrome of *S. oneidensis* MR-1 in which the longest dimension is spanned by a chain of four hemes, Fig. 1. STC presents an excellent *in vitro* system for resolving fundamental and applied aspects of electron transfer in multiheme cytochromes since it is representative in two important aspects. Firstly, each heme has His/His axial ligation. Secondly, the spatial arrangements of neighbouring hemes are those most frequently associated with multiheme cytochromes; the porphyrin ring planes are parallel for STC hemes 2,3 and perpendicular for STC hemes 1,2 and 3,4. Furthermore, STC is soluble, amenable to amino acid substitution and readily purified in the quantities that facilitate biophysical studies [4b-d].

[a] Dr J. H. van Wonderen, Dr D. Li, S. Piper, Dr C. Hall, Dr T. A. Clarke, Dr. N. J. Watmough, Prof. J. N. Butt
School of Chemistry and School of Biology, University of East Anglia, Norwich Research Park, Norfolk, NR4 7TJ (UK)
E-mail: j.butt@uea.ac.uk
[b] Present address: Department of Chemistry, University of Science and Technology of China, Hefei 230026, China and Collaborative Innovation Center of Suzhou Nano Science and Technology, Suzhou 215123, China
[c] Present address: ARC Centre of Excellence in Exciton Science, School of Chemistry, The University of Melbourne, Parkville, Victoria 3010, Australia

Supporting information for this article is given via a link at the end of the document.

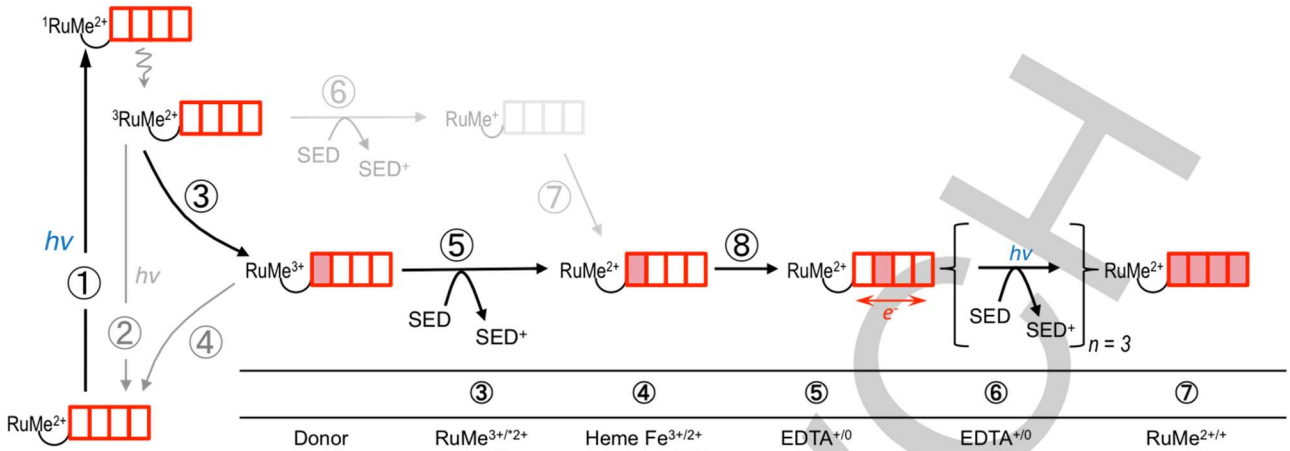

	③	④	⑤	⑥	⑦
Donor E_m (V)	$RuMe^{3+/*2+}$ -0.576	Heme $Fe^{3+/2+}$ -0.200 (-0.050)	$EDTA^{+/0}$ 1.370	$EDTA^{+/0}$ 1.370	$RuMe^{2+/+}$ -1.066
Acceptor E_m (V)	Heme $Fe^{3+/2+}$ -0.200 (-0.050)	$RuMe^{3+/2+}$ 1.524	$RuMe^{3+/2+}$ 1.524	$RuMe^{*2+/+}$ 1.034	Heme $Fe^{3+/2+}$ -0.200 (-0.050)
ΔE_m (V)	0.376 (0.526)	1.724 (1.574)	0.154	-0.336	0.866 (1.016)

Scheme 1. STC-RuMe photochemistry in the presence of a sacrificial electron donor (SED). The four hemes of STC are rectangles: white fill = oxidised, red fill = reduced. Photoreduction of STC-RuMe is a multi-step process: ① photoexcitation of $RuMe^{2+}$ at ≈450 nm forms $^1RuMe^{2+}$ which is followed by rapid conversion to $^3RuMe^{2+}$, ③ oxidative quenching with charge separation by electron transfer to the closest STC heme, ⑤ irreversible oxidation of a SED coupled to reduction of $RuMe^{3+}$, and ⑧ electron migration along the heme chain. Repeated photoreduction produces full, i.e. 4-electron, reduced STC. Processes competing with photoreduction are: ② photoluminescence and ④ charge recombination by electron transfer from reduced heme to $RuMe^{3+}$. For completeness the pathway ⑥ for reductive quenching of $^3RuMe^{2+}$ by SED oxidation followed by ⑦ oxidation of $RuMe^+$ by heme reduction is also shown. Inset: Thermodynamic parameters relevant to the indicated electron transer events with EDTA as SED. E_m values *versus* SHE, 298 K are for the lowest (highest) E_m STC heme [this work], for the Ru(II)-dye in steps ③,④,⑤ are for RuMe [12] and in steps ⑥,⑦ are for Ru(bipyridine)$_3^{2+}$ [18a], the value for $EDTA^{+/0}$ is from [18b].

Here we report engineering STC to act as a phototransducer by converting light to electricity, Fig. 1. Variant forms of STC are labelled with a Ru(bipyridine)$_3^{2+}$ dye photosensitiser that absorbs visible light and injects photoenergised electrons into a terminus of the heme chain. These electrons become trapped in the protein when the oxidised Ru-dye receives electrons from a sacrificial electron donor (SED) and as a consequence STC can accumulate up to four photoenergised electrons. Properties of five Ru-dye labelled STC proteins are presented here and the time courses of cumulative photoreduction are shown to be dependent on the site of Ru-dye attachment, Fig. 1. Our findings are discussed in the context of strategies to engineer efficient coupling of one-electron photochemistry with multi-electron chemical transformations, a major challenge in achieving effective solar chemical transformations [5].

Results and Discussion

Design of photosensitised STC variants. Mononuclear Ru(bipyridine)$_3^{2+}$ complexes are well-characterised photosensitisers with good overall photochemical stability [6]. The metal-to-ligand charge transfer (CT) bands of these dyes are centered at ≈450 nm. Photoexcitation into this charge transfer band, e.g. Scheme 1 ①, produces a singlet state that very rapidly (<psec) forms a longer-lived triplet state. Quenching of the excited triplet state can occur by luminescence, e.g. Scheme 1 ②, producing an emission band with λ_{max} ≈620 nm [7], however the triplet state can also act as a strong oxidant (e.g., ⑥) or reductant (e.g., ③). Indeed, quenching by electron exchange has been reported with a wide-range of materials and molecules with the consequence that Ru(bipyridine)$_3^{2+}$ complexes have been used in dye-sensitized solar cells [8], approaches to solar chemical transformation [9] and studies of intra- and inter-protein electron transfer [10]. The latter is relevant to our work which takes advantage of the pioneering work of Millett and Durham [11] for site-selective labelling of Cys residues with Ru(bipyridine)$_3^{2+}$ dyes. Specifically, we used the thiol reactive photosensitiser RuMeBr (Ru(II)(bipyridine)$_2$(4-bromomethyl-4'-methylbipyridine)) [12] to attach RuMe to a unique Cys introduced to the surface of STC near a terminus of the heme chain, Fig 1.

Crystal structures [4a] of STC were inspected to identify amino acid residues presenting their sidechains on the protein surface near either Heme 1 (Table S1) or Heme 4 (Table S2). Using the empirical forcefield software FoldX-YASARA [13], each of these residues was replaced separately by Cys in the structure [4a] of oxidised STC (pdb accession code 1M1Q) and the impact on STC structural integrity was predicted. From these results (Tables S1,S2) the sites selected for replacement by Cys were those expected to (a) make minimal contribution to STC structural integrity and (b) position RuMe closer to Heme 1 or Heme 4 than any other heme. In the absence of structural models for the RuMe-labelled proteins, the latter property was assessed by the through-space Cys-S to heme-edge distances generated by FoldX-YASARA (Tables S1, S2). After these considerations five sites, Fig. 1, were selected for replacement by Cys, namely, A10 and T23 near Heme 1 and S77, D80 and S87 near Heme 4. The corresponding STC variants, each harbouring a single reactive cysteine and termed STC-10, STC-23 *etc* were purified from *S. oneidensis* MR-1 with the aid of an N-terminal Strep II tag as described below. Residue numbers refer to those of native STC[4a]

for consistency. For comparative purposes, N-terminal Strep II tagged STC having the sequence of native protein, termed STC, was also prepared.

Preparation and spectroscopic characterisation of RuMe-labelled STC proteins. STC proteins were purified from arabinose induced *S. oneidensis* MR-1 strains carrying the corresponding gene on a pBAD-TOPO plasmid as described in the Experimental Section. Briefly, the harvested cells were washed, lysed by French Press and the proteins recovered from cell lysate using a Strep-Tactin XT Superflow column. Material that bound to the column was eluted with biotin and an aliquot exposed to disulphide reducing agent TCEP (1 mM) prior to resolution by denaturing gel electrophoresis. A single broad band of approximately 15 kDa, Fig S1, corresponding to the anticipated size of Strep II tagged STC monomer was revealed for each variant after proteins were visualised by Coomassie stain and heme-based peroxidase activity. LC-MS of each variant revealed a single peak confirming the desired substitution and the presence of four covalently bound hemes, Table 1 and Fig. S2.

Labelling of the purified STC variants was achieved by incubation with a 2-fold excess of RuMeBr for 3-4 hr in the dark at ambient temperature. Subsequent anion exchange chromatography resolved protein eluting more rapidly than the unlabelled counterpart. LC-MS showed the faster eluting material to be protein labelled with a single RuMe (595 Da), Table 1 and Fig. S2, that we term STC-10-RuMe, STC-23-RuMe *etc*. Purity of the labelled proteins was judged to be >95% as LC-MS failed to detect unlabelled proteins.

The electronic absorbance of RuMeBr between 250 and 700 nm contains two major features, Fig. 2 black. The larger band occurs in the UV region (λ_{max} ≈288 nm) with a smaller band at visible wavelengths (λ_{max} ≈460 nm). Neither feature overlaps significantly with those of the STC hemes (Fig. 2 red) which lie between 380-440 nm (Soret-band) and 500-570 nm (α/β- bands) [4a]. For each STC-RuMe protein the electronic absorbance was greater than that of the unlabelled counterpart below ≈350 nm and between 440 - 480 nm, Fig. 2 blue and Fig. S3. Comparison of absorbance for each STC-RuMe protein, the corresponding unlabelled protein and RuMeBr was consistent with the former being labelling by a single RuMe.

The presence of four His/His ligated, and consequently low-spin, hemes in the STC-RuMe proteins was confirmed by their electronic absorbance that was indistinguishable from that of STC (e.g. Fig. 2 and Fig. S3). The Soret maximum was 407 nm for the oxidised proteins. Chemical reduction by sodium dithionite shifted this maximum to 418 nm and was accompanied by the appearance of sharp peaks in the α/β region centered at 522 and 552 nm. There were no signs of features from high-spin heme. For oxidised STC-77-RuMe, further evidence for His/His ligation was provided by room temperature Magnetic Circular Dichroism (MCD) in the near infra-red. MCD resolves ligand-to-metal CT transitions with energies diagnostic of the axial ligands to Fe(III) heme: a pair of bisignate bands for high-spin (CT1 at 800–1300 nm and CT2 at 600–660 nm); a single positive band for each low-spin heme (CTLS at 1000–2500 nm) [14]. For this wavelength range, STC-77-RuMe displayed a single CT-band (Fig. S4) with a maximum at ~1500 nm and an intensity (≈4 M^{-1} cm^{-1} T^{-1}) consistent with four His/His ligated Fe(III) hemes.

Table 1. LC-MS Results for N-terminal Strep II tagged STC Proteins.

	Predicted Mass Prior to Labelling (Da)	Observed Mass Prior to Labelling (Da)	Observed Mass After Labelling (Da)
STC	13 442	13 446	-
STC-10	13 476	13 477	14 071
STC-23	13 444	13 448	14 042
STC-77	13 458	13 462	14 056
STC-80	13 432	13 433	14 028
STC-87	13 558	13 561	14 056

Electrochemical characterisation of STC-RuMe proteins. Redox properties associated with the STC-RuMe proteins were assessed by chemical and electrodic reduction, all potentials reported below are *versus* SHE. Addition of an excess of the mild reductant sodium ascorbate (E_m ≈ -80 mV [15]) produced no reduction as judged by electronic absorbance spectroscopy. In contrast, and as described above Fig. 2 and Fig. S3, complete reduction of all four hemes was observed on addition of the

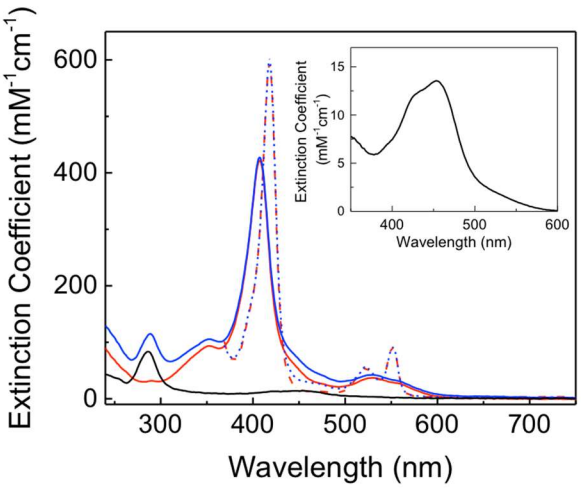

Figure 2. Electronic absorbance of STC-77-RuMe (blue) and STC (red) in the oxidised (continuous lines) and sodium dithionite reduced (broken lines) states. Electronic absorbance of RuMeBr (black) and inset highlighting the charge transfer band. Samples in 20 mM TRIS-HCl, 100 mM NaCl, pH 8.5.

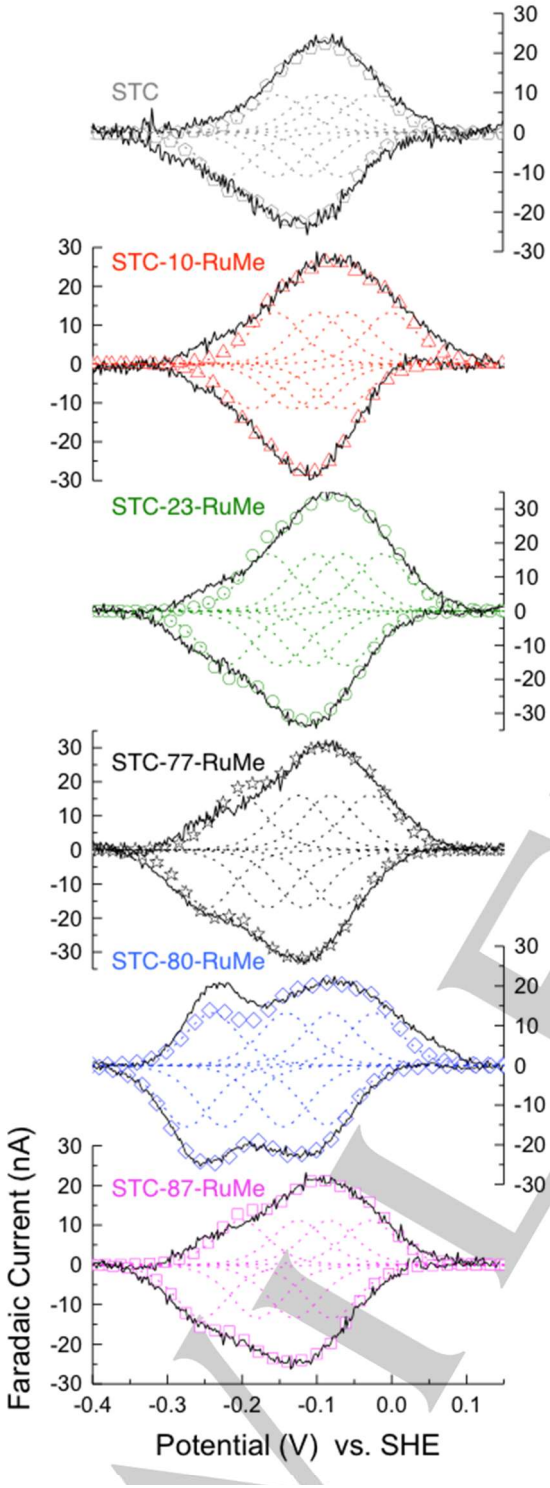

Figure 3. Non-turnover peaks observed in cyclic voltammetry of STC and STC-RuMe proteins adsorbed on graphite electrodes. Measured currents (continuous lines) were modelled as the sum (symbols) of four equal contributions (dashed lines) from single-electron Nernstian centres. Experiments performed with a scan rate of 10 mV s^{-1} in 50 mM HEPES, 50 mM NaCl, pH 7.5, at room temperature.

stronger reductant sodium dithionite (E_M < -500 mV at pH 8.5, 25 °C [16]).

In view of this behaviour, greater insight into the redox properties was afforded by cyclic voltammetry between +100 and -400 mV with each protein adsorbed as an electroactive film on graphite electrodes. The voltammetric responses for STC and proteins labelled with RuMe at position 10, 23, 77 and 87 were very similar, Fig. 3, indicating the hemes occupy comparable environments in these proteins. In the simplest case, cyclic voltammetry of a single, isolated one-electron redox couple under the experimental conditions used here will produce symmetrical peaks centered on E_m, with half-height widths of ≈100 mV and having positive current for oxidation and negative current for reduction. The peaks arising from the STC proteins have structure and half-height widths >120 mV indicative of overlapping contributions from hemes with different E_m values. Indeed, each of the peaks was well-described by the sum of four equal Nernstian contributions from independent one-electron redox centres, e.g. dashed lines Fig. 3. Averaging the peak potentials from modelling the oxidative and reductive peaks of the STC-RuMe proteins labelled at positions 10, 23, 77 and 87 gave E_m values of ≈ -45, -95, -135, and -200 mV which are similar to those reported previously for STC [4d].

The voltammetric response of STC-80-RuMe has a different shape to those of the other proteins in that the peaks have greater area at more negative potentials, Fig. 3. Modelling the current-potential profiles as described above gave E_m values of ≈-55, -112, -180, and -255 mV that extended to more negative values. Thus, at least one STC-80-RuMe heme as a different environment to that experienced in the other proteins. Some insight into the possible origin(s) of this behaviour was provided by studying STC-80. The voltammetric response of STC-80, Fig. S5, was comparable to that of STC-80-RuMe and different to those of the other (un)labelled proteins. Thus, substitution of Asp80 by Cys, rather than RuMe labelling of STC-80, is responsible for changing the heme reduction potentials. Replacing Asp80 by Cys is expected to remove negative charge and raise heme reduction potentials. Therefore, the lower E_m values that are observed may arise from an increase in heme(s) solvent exposure [17].

Photoluminescence (PL) of STC-RuMe proteins. Having characterised structural and thermodynamic properties of the STC-RuMe proteins, evidence for light-driven electron transfer from $^3RuMe^{2+}$ to STC hemes was sought from PL of the RuMe-dye, Scheme 1 ②. PL quenching by FRET is unlikely due to poor spectral overlap of the RuMe emission and heme absorbance (compare Fig. 2 with Fig. 4). However, oxidative quenching of $^3RuMe^{2+}$ by charge separation, Scheme 1 ③, to form $RuMe^{3+}$ and reduced heme is thermodynamically possible, Scheme 1 inset [12, 18]. If oxidative quenching is competitive with PL the STC-RuMe proteins should display lower PL intensity than RuMe-labelled bovine serum albumin (BSA). This is because there are no cofactors in BSA so $^3RuMe^{2+}$ quenching by electron transfer is not possible. Preparation and characterisation of BSA labelled with one RuMe, termed BSA-RuMe, is described in the Experimental Section.

When excited at 460 nm, anaerobic solutions of the STC-RuMe and BSA-RuMe proteins display emission bands, Fig. 4, spanning from ≈550 to 750 nm with a maximum at ≈625 nm. However, emission intensity from the STC-RuMe proteins is at most 3% of that from BSA-RuMe. The results indicate oxidative quenching by electron transfer from $^3RuMe^{2+}$ to the neighbouring STC heme is competitive with PL. Quenching is greatest for STC-77-RuMe indicating fastest charge separation in this protein. Residue 77 is unique in being the only one of our labelling sites to lie within a CxxCH heme binding motif. In this motif the Cys residues form thioether bonds to the porphyrin ring and the His is a proximal ligand to Fe. STC Heme 4 is attached to a CESCH motif containing residue 77 (underlined). When the Cys that replaces Ser77 is labelled with RuMe only 7 bonds separate the RuMe and Heme 4. Faster charge separation in this, than the other STC-RuMe proteins is consistent with ultra-fast transient absorbance [19] of RuMe-labelled cytochrome c_7 proteins that revealed much faster charge separation for RuMe introduced in a heme binding motif (CKKCH) than at other positions.

An additional feature of the PL spectra is worthy of note. Specifically, STC-80-RuMe gives an emission band with considerable intensity at lower wavelengths than the corresponding bands from the other proteins. As photoexcited $Ru(bipyridine)_3^{2+}$ complexes emit at shorter wavelengths when in a rigid matrix rather than fluid solution [20] it seems likely that some population of the dye associated with STC-80-RuMe, and not the other proteins, is at least partially embedded in the protein structure and shielded from solvent. Such behaviour could be linked to the lower heme E_m values described above for STC-80-RuMe and the possibility that heme(s) experience different environments in this protein when compared to others.

Photoreduction of STC-RuMe proteins. In the PL experiments described above, the $RuMe^{3+}$-STC^- produced by oxidative quenching, Scheme 1 ③, undergoes charge recombination ④ which returns the ground state $RuMe^{2+}$-STC. As a consequence STC does not accumulate electrons in that experiment. However, photoexcited electrons should accumulate in STC if reduction of

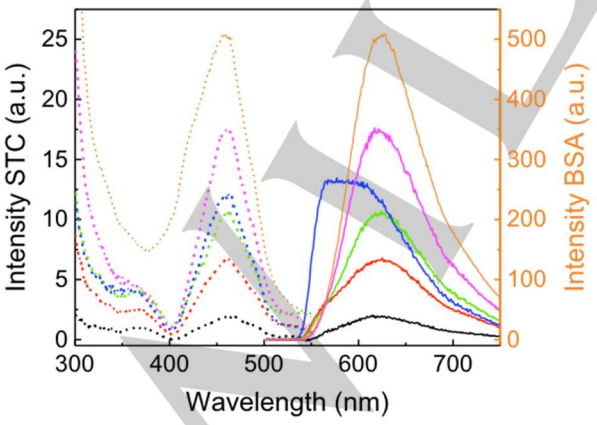

Figure 4. Photoluminescence of STC-RuMe proteins and BSA-RuMe. Excitation (emission at 620 nm) as dashed lines and emission (excitation at 460 nm) as solid lines for STC-10-RuMe (red), STC-23-RuMe (green), STC-77-RuMe (black), STC-80-RuMe (blue), STC-87-RuMe (magenta) and BSA-RuMe (orange). STC-RuMe proteins (~8 μM) and BSA-RuMe (~2.5 μM) in anaerobic, 20 mM Tris, 100 mM NaCl, pH 8.5.

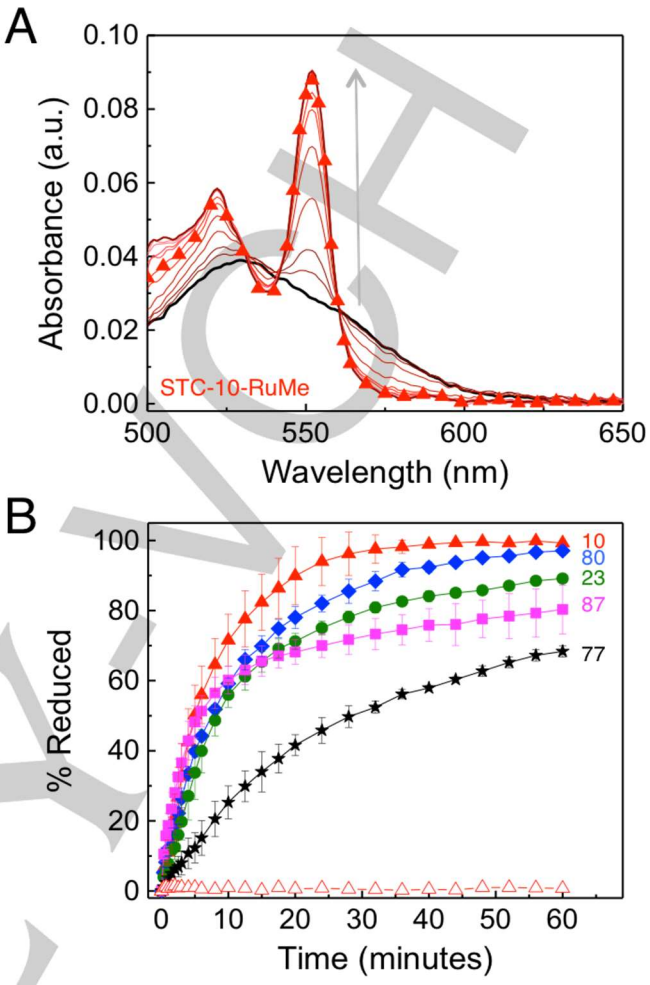

Figure 5. Photoreduction of STC-RuMe proteins. A. Electronic absorbance of STC-10-RuMe (1 μM) after 0 (black), 1, 2, 4, 8, 15, 20, 28 (thick red) min irradiation with 455 nm light (60 Wm^{-2} power at the sample) followed by addition of excess sodium dithionite (triangles). The anaerobic sample contained 1 μM protein in 20 mM Tris, 100 mM NaCl, pH 8.5 with 50 mM EDTA. B. Time course for heme reduction in STC-RuMe proteins as indicated (filled symbols), conditions as for A. Time course for photoreduction of STC-10-RuMe in the absence of EDTA (open red triangles), all other conditions as for A.

$RuMe^{3+}$ by EDTA as SED [21], Scheme 1 ⑤, occurs at sufficient rate to compete with charge recombination. To assess this possibility anaerobic solutions containing EDTA and STC-RuMe were irradiated with blue light (λ~452 nm) as described in Experimental Section. Heme oxidation state was monitored by electronic absorbance of the heme α-/β-bands, e.g. Fig. 5A. Measurement of the Soret band was precluded as a notch-filter was used to remove wavelengths between ≈420 and 530 nm that would photoexcite RuMe.

Spectra recorded during 60 min irradiation of STC-10-RuMe, Fig. 5A, revealed the formation of sharp, relatively intense features centred on 522 and 552 nm that were indicative of formation of ferrous heme. There was no further spectral change when the blue light was removed for 10 min demonstrating that the product(s) [21] of EDTA oxidation fail to oxidise reduced heme. Similar results were obtained with the additional STC-RuMe

proteins, Fig. S6, revealing light-driven electron accumulation in all samples. Photoreduction was found to be significantly faster in the presence of EDTA than other sacrificial electron donors including aniline, *p*-anisidine and triethanolamine.

Time courses comparing photoreduction of the five STC-RuMe proteins with EDTA as sacrificial electron donor are presented in Fig. 5B. The data were collected in the following way. Samples were irradiated continuously for 60 min during which time spectra were collected at the desired time points, then, an excess of the chemical reductant sodium dithionite was added to ensure complete protein reduction and the spectrum of the sample re-measured. The absorbance at 552 nm was compared to that obtained on full chemical reduction of the sample to allow the data to be presented as % reduction versus irradiation time, Fig. 5B, and revealing clear differences in the behaviours of the proteins. The initial rate of photoreduction is significantly less for STC-77-RuMe than for the other proteins. For the proteins labelled with RuMe at positions 10, 23, 80 and 87 the times taken to accumulate more than 2 electrons (i.e. display 60 to 100% reduction) vary considerably. This process occurs most rapidly for STC-10-RuMe.

It seems reasonable to assume equivalent rates of photoexcitation, Scheme 1 ①, by the STC-RuMe proteins. Similar rates are also likely for the corresponding PL, Scheme 1 ②, with frequencies of ≈ 5 x 10^6 s^{-1} reported previously [12]. As a consequence, the different time courses observed for cumulative photoreduction must arise from protein specific differences in the rate(s) of the additional reactions of Scheme 1, both productive and off-pathway. We first considered whether oxidative quenching of the photoexcited dye Scheme 1 ③, as demonstrated above, was accompanied by reductive quenching Scheme 1 ⑥. The latter step is predicted to be endergonic with EDTA as SED, Scheme 1 inset, and the measured PL of BSA-RuMe was found to be unchanged in the presence of EDTA, Fig. S8. Thus, it is unlikely that reductive quenching operates in our experiments. In accord with Scheme 1, no photoreduction was detected with unlabelled proteins, or in the absence of blue light (Fig. S7A) or EDTA (Fig. 5B open triangles and Fig. S7, B-F).

Given that charge separation is fastest in STC-77-RuMe, why does this protein display the slowest initial rate of cumulative photoreduction? The reason should lie in the fate of the $RuMe^{3+}$-STC^{n-} species, specifically, the outcome of the competition between irreversible EDTA oxidation trapping electrons in the heme chain (Scheme 1 ⑤) and non-productive charge recombination (Scheme 1 ④). Studies of EDTA oxidation by $^3Ru(bipyridine)_3^{2+}$ show this process can occur with a second order rate constant of 2 x 10^6 M^{-1} s^{-1} [22]. Charge recombination is predicted to be fastest in STC-77-RuMe as this process is favoured by the same parameters that favour charge separation. As a consequence the net rate of irreversible EDTA oxidation is predicted to be slowest for STC-77-RuMe explaining why this protein has the lowest initial rate for cumulative photoreduction.

For light-driven electron accumulation in STC, electron migration away from the RuMe-injection site along the heme chain is required. As a consequence the photoreduction time courses should reflect interplay of the site of electron injection and the rate(s) of subsequent electron distribution along the heme chain. Experiments [23] and computational chemistry [24] have shown that inter-heme electron transfer within STC occurs at rates > 10^4 s^{-1} and so on a timescale much faster than STC cumulative photoreduction. In these circumstances heme E_M values will define the distribution of photo-accumulated electrons across the heme chain. Previous studies of native STC at alkaline pH [4b, 23a] made use of protein NMR to conclude that Hemes 3 and 4 are predominantly Fe(II) in the two-electron (50%) reduced protein and that Hemes 2, 3 and 4 are predominantly Fe(II) in the three-electron (75%) reduced protein. Making the reasonable assumption that the structure and thermodynamics properties of native STC are similar to those of the protein labelled at residues 10, 23, 77 and 87, then cumulative photoreduction by light-driven electron transfer is expected to occur more readily when the Ru-dye injects electrons into Heme 1 rather than Heme 4. This can explain why photo-reduction of > 2 hemes is faster for STC-10-RuMe and STC-23-RuMe than for STC-87-RuMe and STC-77-RuMe. Clearly additional factors contribute to the differences noted for photoreduction of the proteins with RuMe near the same heme and these may be related to the different PL properties of the individual proteins.

Electron injection into Heme 4 is also expected for STC-80-RuMe. For this protein the fast rate of complete photoreduction is presumably a consequence of its different structural and electrochemical properties as noted above. From the perspective of biotechnology the behaviour of this protein is significant because it suggests the system can retain the properties of a molecular wire despite perturbations to the natural form.

Prospects for photosensitised multiheme cytochromes in photocatalysis. Sunlight is our most abundant energy source with enormous potential as a clean and economical energy supply. Photovoltaics (solar panels) demonstrate scalable and cost-efficient conversion of solar energy to electricity. However, the development of scalable and cost-efficient routes to light-driven chemical synthesis, whether of fuels, commodity or fine chemicals, represents a major challenge in moving to a circular economy [5]. Natural photosynthesis harnesses solar energy to drive chemical transformations and provides inspiration for solar chemicals production. Algae can provide high fuel yields and photosynthetic bacteria engineered to develop alternatives to C_3 and C_4 fixation. Existing technologies for photovoltaics and electrolysis cells can be coupled for light-driven chemical catalysis. Furthermore, light-absorbing chromophores that generate photoenergised electrons (holes) can be coupled to electrocatalysts that use the energised electrons (holes) to make fuels or valued chemicals. In the latter context the electron transfer properties of redox proteins and enzymes have an important role to play in guiding concepts and design strategies for robust future technologies [25].

Previous studies have demonstrated that Ru-photosensitised proteins can act as biohybrids using sunlight for direct chemical catalysis. A Ru-dye photosensitiser coupled to the molybdenum-iron-protein of nitrogenase supported photocatalytic reduction of protons and acetylene [26]. Synthetic electrocatalysts were integrated with a series of RuMe-photosensitised ferredoxins and flavodoxins that performed light-driven H_2

evolution [27]. The biohybrids stabilised the electrocatalysts in aqueous solution allowing proton reduction across a wide pH range. Furthermore, the ferredoxin provided an electron holding station in a manner analogous to the use of TiO_2 nanoparticles [9b] for collecting electrons (holes) from photoexcited Ru-dyes until they are needed for catalysis. The work presented here complements those observations by demonstrating that RuMe-labelled STC transduces visible light to electricity by acting as a biohybrid with the capacity to store up to 4 electrons.

Moving forward, and from the perspectives of both solar chemicals production and molecular electronics, it is significant that the light-stimulated electronic properties of our RuMe-STC biohybrids are dependent on the site of RuMe-labelling. The time course for cumulative photoreduction of STC-87-RuMe illustrates a resistance to accumulating >2e^- whereas STC-10-RuMe rapidly accumulates 4e^-. Thus, while STC-10-RuMe acts as a light driven molecular wire, the properties of STC-87-RuMe are more akin to those of a light-driven resistor and we propose these behaviours result from the interplay between the site of electron injection and the distribution of reduction potentials along the heme chain.

We consider there to be much scope for engineering these proteins, and homologs, to achieve diverse and bespoke electrical properties. For example, longer-lived charge separation and faster electron migration from the site of photoenergised electron injection may be achieved by optimal redox landscape in the heme chain and/or injection into heme with its porphyrin ring parallel, rather than perpendicular, to its neighbour [24, 28]. Futhermore, the 2- and 3-dimensional heme arrays of larger multiheme cytochromes [29] may display additional functionalities, for example providing light-driven molecular junction boxes. Future work in our laboratory aims to explore these possibilities and resolve the molecular determinants of electron transfer in photosensitised-multiheme cytochromes such as the STC-RuMe proteins described here.

Experimental Section

Protein Engineering and Purification. Bacterial strains and plasmids used in this study are listed in Table S4 with primers (Eurofins) detailed in Table S5. Native and variant STC (CctA) proteins were produced with an N-terminal Strep II-tag to assist purification. The corresponding genes were carried on a pBAD202/D-TOPO plasmid to allow their expression in *S. oneidensis* MR-1 (MR-1) from an L-arabinose inducible promoter. The gene, Fig. S9, for the tagged native STC encoded for the Strep II-tag, flanked on either side by a spacer of two amino acids, between the sequence (locus tag SO_2727) for the mature STC and that of its N-terminal signal peptide for secretion via the Sec pathway to the periplasm. A ribosomal binding site for the thioredoxin gene of the pBAD202 plasmid was positioned upstream of this gene and appropriately positioned stop codons precluded peptide extensions that are otherwise intrinsic to the pBAD system. The gene was constructed in a kanamycin resistant pUC57 cloning vector (Genscript) and the resulting construct, pJvW002, carried a 5'-CACC to allow for directional cloning into pBAD/D-TOPO.

The desired region of pJvW002 was amplified by PCR (Phusion Flash High-Fidelity PCR Master Mix, ThermoFisher Scientific), purified and inserted into pBAD202/D-TOPO plasmid using the pBAD202 Directional TOPO Expression Kit (ThermoFisher Scientific). For introducing surface cysteines into STC the resulting plasmid, pJvW003, was used as the template and the desired mutations were introduced by PCR with appropriate primers. The resulting plasmids (pJvW003-008) were introduced into chemically competent *E. coli* OneShot TOP10 cells and the transformed cells streaked onto LB agar plates containing kanamycin (50 μg mL^{-1}). The purified plasmids were transformed by electroporation into MR-1 to create strains JvW003-008 and successful incorporation of the desired plasmids confirmed by Sanger DNA sequencing (Eurofins).

For purification of the Strep-tagged STC proteins, 100 mL of LB media containing 30 μg mL^{-1} kanamycin was inoculated (1%) with the desired strain and grown aerobically overnight. These cultures provided inocula (2 %) for 5 L of M72 media [30] supplemented with 20 mM lactate, 30 mM fumarate and 25 mM HEPES, 30 μg ml^{-1} kanamycin at pH 7.8. Cells were grown at 30°C without shaking and expression of the STC genes induced after ~8 hours (OD ~0.3) by addition of 10 mM L-arabinose. Cells were harvested 14 hours after induction by centrifugation (3603 x*g* for 15 min, 4°C) and resuspended in 25 ml of 50 mM NaH_2PO_4, 300 mM NaCl, pH 8.0 containing 1 mM DTT, 5 % glycerol, 1 x protease inhibitor tablet (SIGMAFAST Protease Inhibitor tablet, EDTA-free - Sigma Aldrich)) and 50 μL biotin blocking solution (ThermoFisher Scientific). The suspension was lysed by passage through a French Press (1000 PSI) and subjected to ultracentrifugation (164,684 x*g* for 1 hr, 4°C) to remove membranes and cell debris. The supernatant was applied to a Strep-tactin XT gravity flow Superflow column (5 mL, IBA Solutions for Life Sciences), pre-equilibrated in 50 mM NaH_2PO_4, 300 mM NaCl, pH 8.0, at a flow rate of approximately 2 mL min^{-1} using a WET FRED system (IBA Solutions for Life Sciences). Loosely bound materials were removed by washing the column with 50 mM NaH_2PO_4, 300 mM NaCl, pH 8.0 and pure Strep-tagged STC proteins eluted with 50 mM NaH_2PO_4, 300 mM NaCl, pH 8.0 containing 20 mM biotin [31]. Samples were exchanged into 20 mM TRIS-HCl, pH 7.5 buffer by centrifugal filtration (Centricon/Microcon 5 kDa cutoff) and their purity and identity assessed by a combination of denaturing gel electrophoresis, electronic absorbance spectroscopy and LC-MS. Purified proteins were stored as frozen aliquots at -80 °C. Concentrations of the STC proteins were determined by electronic absorbance of the air-equilibrated (oxidized) forms using $\varepsilon_{407\,nm}$ = 422 mM^{-1} cm^{-1} or $\varepsilon_{552\,nm}$ = 29.1 mM^{-1} cm^{-1}.

RuMe labelling. Labelling of STC cysteine variants with the Ru-phototrigger was performed in 20 mM Tris-HCl, pH 7.5 after reduction of any disulphide bonds present in the samples. Reduction of the proteins (50 to 100 μM, approx. 3.5 mL) was performed by addition of an approx. 15-fold excess of TCEP (tris-(2-carboxyethyl)phosphine). After 20 min. reaction the products were separated from reduced protein by centrifugal filtration giving a sample (50 to 100 μM, approx. 3.5 mL) to which a 2-fold molar excess of Ru(II)(4-bromomethyl-4'-methylbipyridine)$(bipyridine)_2(PF_6)_2$ (HetCat Switzerland) was immediately added from a stock solution of approx 30 mM in DMSO ($\varepsilon_{452\,nm}$ = 13.5 mM^{-1} cm^{-1} [12]). The sample was shaken gently for 3 to 4 hr in the dark at ambient temperature.

Purification of RuMe-labelled protein was by anion exchange chromatography. Samples were loaded (2 mL min^{-1}) onto a Q-Sepharose column (5 mL, GE Healthcare, Sigma Aldrich) that had been pre-equilibrated with Buffer A (20 mM TRIS-HCl, pH 7.5 buffer). Any unbound RuMe was washed off using buffer A, until there was no RuMe absorbance at 280 nm, after which the column was equilibrated to 5 % Buffer B (20 mM TRIS-HCl, 1 M NaCl, pH 7.5 buffer). Unbound RuMe was retained for safe disposal. Proteins were eluted with a gradient of 5-30 % Buffer B, collecting 1 ml fractions and monitoring at 280 nm. RuMe-labelled STC variants eluted between 14-16% conductivity and before unlabelled STC at 18-20 % conductivity. LCMS confirmed labelling by a single RuMe group. After mixing Strep II-tagged wild type STC with RuMeBr there was no evidence for reaction between the protein and the dye (data not shown).

This was as expected given that all Cys in Strep II-tagged wild type STC are found in the CxxCH heme binding motifs.

Bovine serum albumin (Sigma-Aldrich) was dissolved in 20 mM TRIS-HCl, 100 mM NaCl, pH 8.5. Labelling was performed using 5-fold excess RuMe label (4ºC, 24 hours) which gave 75 % labelling efficiency. Excess label was removed by anion exchange chromatography and protein characterised by electronic absorbance spectroscopy (43,824 $M^{-1}cm^{-1}$ at 279 nm [32]) and LC-MS where the observed mass of BSA was 66429 Da (predicted 66463 Da) and of BSA-RuMe was 67023 Da (predicted 67058 Da).

Mass spectrometry (LC-MS) methods. Starting concentrations of ~0.4 mg ml^{-1}; ~30 µM NSTC variants ± RuMe were used for the LC-MS. Samples were then diluted to (0.04 mg ml^{-1}; ~3 µM) with an aqueous mixture of 1% (v/v) acetonitrile, 0.3% (v/v) formic acid, and loaded onto a ProSwift RP-1S column (4.6 x 50mm) (Thermo Scientific) on an Ultimate 3000 uHPLC system (Dionex, Leeds, UK). Bound proteins were eluted (0.2 ml min^{-1}) using a linear gradient (15 min) from 2% to 100% (v/v) acetonitrile, 0.1% (v/v) formic acid. The eluent was continuously infused into a Bruker microQTOF-QIII mass spectrometer, running Hystar (Bruker Daltonics, Coventry, UK)), using positive mode electrospray ionisation (ESI). Compass Data Analysis, with Maximum Entropy v1.3, (Bruker Daltonics, Coventry) was used for processing of spectra under the LC peak. The mass spectrometer was calibrated with ESI-L tuning mix (Agilent Technologies).

Optical Spectroscopies & Photoreduction. Photoreduction experiments were performed in degassed buffer (20 mM Tris, 100 mM NaCl, 50 mM EDTA, pH 8.5) and the protein concentration was 1 µM unless otherwise stated. Spectra were recorded in SOG cuvettes in a Biochrom WPA Biowave II Diode-array UV/Vis spectrophotometer under an N_2 atmosphere. An Omega Optical 475RB Notch filter was used to prevent photoexcitation of RuMe by the spectrophotometer. The light source for photoreduction was a Thorlabs mounted LED (λ_{max} 455 nm) equipped with a collimator adapter. The excitation intensity at the sample was ≈ 60 W m^{-2}. Samples were irradiated continuously from above and spectra taken at given times. The percentage of hemes that were reduced was quantified using the baseline-corrected absorbance of the heme α-band at 552 nm. The absorbance at time 0 was taken to be the oxidised state (0%) and the fully reduced state was obtained at the end of the experiment by addition of excess of sodium dithionite solution.

Photoluminescence. Photoluminescence intensity measurements were recorded on STC-RuMe proteins (≈ 8 µM) and BSA-RuMe (≈ 2.5 µM) in anaerobic 20 mM TRIS, 100 mM NaCl, pH 8.5 using acid-washed quartz fluorescence cuvettes. Emission spectra were recorded using an excitation wavelength of 460 nm, excitation spectra were recorded using an emission wavelength of 620 nm. Measurements were made on a Cary Eclipse Fluorescence Spectrophotometer with an excitation slit width of 20 nm, an emission slit width of 10 nm and the PMT detector voltage set to medium.

Protein Film Voltammetry. Experiments employed a three-electrode cell configuration placed inside a Faraday cage housed in a N_2-filled chamber with atmospheric O_2 < 5 ppm as described previously [33]. The cell employed an Ag/AgCl (saturated KCl) reference electrode, and potentials are reported with respect to the Standard Hydrogen Electrode following addition of 197 mV to the measured potential. A pyrolytic graphite edge working electrode of 3-mm diameter was polished immediately prior to use with an aqueous slurry of 0.3 µm Al_2O_3, sonicated, rinsed, and dried with a tissue. The freshly polished electrode was then taken into the N_2-chamber together with aliquots of STC protein (60-120 µM) and co-adsorbant neomycin (5 mM). Immediately, 5 µL STC followed by 5 µL neomycin were drawn into a Hamilton syringe and placed on the electrode surface. After ~20 s excess solution was removed from the electrode with a tissue, rinsed with 50 mM HEPES, 50 mM NaCl, pH 7.5 and placed into the electrochemical cell.

Cyclic voltammetry was performed with an Autolab PGSTAT30 under the control of NOVA software. To define the Faradaic currents due to STC oxidation/reduction, the current recorded with a 'bare' electrode was used as a guide for using NOVA to substract an appropriate baseline from the voltammetric data. The Faradaic currents were fitted to the sum of the 4 equal contributions from isolated, n = 1 redox centres with the equation:

$$Faradaic\ current = \sum_{i=1}^{4} \frac{X(\exp(F(\frac{E-E_i}{RT})))}{(1+\exp(F(E-\frac{E_i}{RT})))^2} \quad (1)$$

where E is the sample potential, E_i the reduction potential, R the gas constant, F the Faraday constant and T absolute temperature and X scales the calculated current to the magnitude measured experimentally. The four E_i values from each peak were paired, from highest to lowest value and averaged to describe the four E_M values reported in the main text.

Acknowledgements

We would like to thank Jochen Blumberger, Antoine Carof, Xiuyun Jiang, Steve Meech amd John Fielden for insightful discussions. We are grateful to assistance from Simone Payne for protein purifcation, Jason Crack for LC-MS, Myles Cheesman and Justin Bradley for MCD, Marcus Edwards for help with molecular biology, Jack McLeish for initial photoreduction studies and the EPSRC UK National Mass Spectrometry Facility at Swansea University for characterisation of RuMeBr. Funding was from the UK Engineering and Physical Sciences Research Council (EP/M001989/1, EP/N033647/1 and the Biotechnology and Biological Sciences Research Council (BB/L022176/1, BB/K009885/1 and Doctoral Training Partnership PhD studentship to SEHP). DL is grateful to the Collaborative Innovation Center of Suzhou Nano Science and Technology (NANO-CIC) in Chinais Collaborative Academic Training Program for Post-doctoral Fellows. JNB acknowledges a Royal Society Leverhulme Trust Senior Research Fellowship.

Keywords: small tetraheme cytochrome (STC) • *Shewanella oneidensis* • electron transfer • Ruthenium tris bipyridine • photocatalysis

Abbreviations: BSA, bovine serum albumin; CT, charge transfer, LC-MS, liquid chromatography-mass spectrometry; MCD, magnetic circular dichroism; PL, photoluminescence; RuMe, Ru(II)(bipyridine)$_2$(4-methylene-4'-methylbipyridine); RuMeBr, Ru(II)(bipyridine)$_2$(4-bromomethyl-4'-methylbipyridine); SHE, standard hydrogen electrode; STC, small tetraheme cytochrome (CctA) from S. oneidensis MR-1; TCEP, tris-(2-carboxy ethyl) phosphine.

References

[1] a) D. R. Lovley, *Annual Review of Microbiology* **2012**, *66*, 391-409; b) L. Shi, H. Dong, G. Reguera, H. Beyenal, A. Lu, J. Liu, H.-Q. Yu, J. K. Fredrickson, *Nature Reviews Microbiology* **2016**, *14*, 651-662; c) A. Kumar, L. H.-H. Hsu, P. Kavanagh, F. Barrière, P. N. L. Lens, L. Lapinsonnière, J. H. Lienhard V, U. Schröder, X. Jiang, D. Leech, *Nature Reviews Chemistry* **2017**, *1*, 0024.

[2] a) M. Breuer, K. M. Rosso, J. Blumberger, J. N. Butt, *Journal of The Royal Society Interface* **2015**, *12*; b) R. Kumar, L. Singh, A. W. Zularisam, *Renewable and Sustainable Energy Reviews* **2016**, *56*, 1322-1336; c) K. Inoue, X. Qian, L. Morgado, B.-C. Kim, T. Mester, M. Izallalen, C. A. Salgueiro, D. R. Lovley, *Applied and environmental microbiology* **2010**, *76*, 3999-4007; d) G. F. White, M. J. Edwards, L. Gomez-Perez, D. J. Richardson, J. N. Butt, T. A. Clarke, in *Advances in Microbial Physiology, Vol. 68* (Ed.: R. K. Poole), Academic Press, **2016**, pp. 87-138.

[3] a) S. Kato, *Microbes and Environments* **2015**, *30*, 133-139; b) N. Schuergers, C. Werlang, C. M. Ajo-Franklin, A. A. Boghossian, *Energy & Environmental Science* **2017**, *10*, 1102-1115; c) K. Sasaki, D. Sasaki, K. Kamiya, S. Nakanishi, A. Kondo, S. Kato, *Current Opinion in Biotechnology* **2018**, *50*, 182-188.

[4] a) D. Leys, T. E. Meyer, A. S. Tsapin, K. H. Nealson, M. A. Cusanovich, J. J. Van Beeumen, *Journal Biological Chemistry* **2002**, *277*, 35703-35711; b) B. M. Fonseca, I. H. Saraiva, C. M. Paquete, C. M. Soares, I. Pacheco, C. A. Salgueiro, R. O. Louro, *Journal Biological Inorganic Chemistry* **2009**, *14*, 375-385; c) C. M. Paquete, R. O. Louro, *Dalton transactions* **2010**, *39*, 4259-4266; d) Y. Qian, C. M. Paquete, R. O. Louro, D. E. Ross, E. Labelle, D. R. Bond, M. Tien, *Biochemistry* **2011**, *50*, 6217-6224.

[5] a) D. Gust, T. A. Moore, A. L. Moore, *Accounts of Chemical Research* **2009**, *42*, 1890-1898; b) J. H. Montoya, L. C. Seitz, P. Chakthranont, A. Vojvodic, T. F. Jaramillo, J. K. Nørskov, *Nature Materials* **2016**, *16*, 70; c) C. Gao, J. Wang, H. Xu, Y. Xiong, *Chemical Society reviews* **2017**, *46*, 2799-2823.

[6] a) V. Balzani, A. Juris, *Coordination Chemistry Reviews* **2001**, *211*, 97-115; b) Q. Lam, M. Kato, L. Cheruzel, *Biochimica et Biophysica Acta (BBA) - Bioenergetics* **2016**, *1857*, 589-597.

[7] a) N. H. Damrauer, G. Cerullo, A. Yeh, T. R. Boussie, C. V. Shank, J. K. McCusker, *Science* **1997**, *275*, 54-57; b) A. Cannizzo, F. v. Mourik, W. Gawelda, G. Zgrablic, C. Bressler, M. Chergui, *Angewandte Chemie International Edition* **2006**, *45*, 3174-3176.

[8] A. Hagfeldt, M. Grätzel, *Accounts of Chemical Research* **2000**, *33*, 269-277.

[9] a) M. D. Kärkäs, E. V. Johnston, O. Verho, B. Åkermark, *Accounts of Chemical Research* **2014**, *47*, 100-111; b) J. Willkomm, K. L. Orchard, A. Reynal, E. Pastor, J. R. Durrant, E. Reisner, *Chemical Society reviews* **2016**, *45*, 9-23.

[10] a) H. B. Gray, J. R. Winkler, *Proceedings of the National Academy of Sciences of the United States of America* **2005**, *102*, 3534-3539; b) L. Geren, B. Durham, F. Millett, *Methods in enzymology* **2009**, *456*, 507-520.

[11] F. Millett, B. Durham, *Biochemistry* **2002**, *41*, 11315-11324.

[12] L. Geren, S. Hahm, B. Durham, F. Millett, *Biochemistry* **1991**, *30*, 9450-9457.

[13] a) J. Van Durme, J. Delgado, F. Stricher, L. Serrano, J. Schymkowitz, F. Rousseau, *Bioinformatics* **2011**, *27*, 1711-1712; b) J. Schymkowitz, J. Borg, F. Stricher, R. Nys, F. Rousseau, L. Serrano, *Nucleic Acids Res* **2005**, *33*, W382-388; c) E. Krieger, G. Koraimann, G. Vriend, *Proteins* **2002**, *47*, 393-402; d) R. Guerois, J. E. Nielsen, L. Serrano, *Journal of Molecular Biology* **2002**, *320*, 369-387.

[14] M. R. Cheesman, C. Greenwood, A. J. Thomson, *Advances in Inorganic Chemistry* **1991**, *36*, 201-255.

[15] J. S. Fruton, *Journal of Biological Chemistry* **1934**, *105*, 79-85.

[16] S. G. Mayhew, *European Journal of Biochemistry* **1978**, *85*, 535-547.

[17] F. A. Tezcan, J. R. Winkler, H. B. Gray, *Journal of the American Chemical Society* **1998**, *120*, 13383-13388.

[18] a) D. P. Rillema, G. Allen, T. J. Meyer, D. Conrad, *Inorganic chemistry* **1983**, *22*, 1617-1622; b) A.-M. Manke, K. Geisel, A. Fetzer, P. Kurz, *Physical Chemistry Chemical Physics* **2014**, *16*, 12029-12042.

[19] O. Kokhan, N. S. Ponomarenko, P. R. Pokkuluri, M. Schiffer, K. L. Mulfort, D. M. Tiede, *J Phys Chem B* **2015**, *119*, 7612-7624.

[20] a) P. Innocenzi, H. Kozuka, T. Yoko, *The Journal of Physical Chemistry B* **1997**, *101*, 2285-2291; b) E. L. Sciuto, M. F. Santangelo, G. Villaggio, F. Sinatra, C. Bongiorno, G. Nicotra, S. Libertino, *Sensing and Bio-Sensing Research* **2015**, *6*, 67-71.

[21] Y. Pellegrin, F. Odobel, *Comptes Rendus Chimie* **2017**, *20*, 283-295.

[22] a) D. Miller, G. McLendon, *Inorganic chemistry* **1981**, *20*, 950-953; b) D. R. Prasad, K. Mandal, M. Z. Hoffman, *Coordination Chemistry Reviews* **1985**, *64*, 175-190.

[23] a) E. Harada, J. Kumagai, K. Ozawa, S. Imabayashi, A. S. Tsapin, K. H. Nealson, T. E. Meyer, M. A. Cusanovich, H. Akutsu, *FEBS Letters* **2002**, *532*, 333-337; b) C. M. Paquete, I. H. Saraiva, E. Calçada, R. O. Louro, *Journal of Biological Chemistry* **2010**, *285*, 10370-10375.

[24] X. Jiang, Z. Futera, M. E. Ali, F. Gajdos, G. F. von Rudorff, A. Carof, M. Breuer, J. Blumberger, *Journal of the American Chemical Society* **2017**, *139*, 17237-17240.

[25] a) A. Bachmeier, F. Armstrong, *Current opinion in chemical biology* **2015**, *25*, 141-151; b) T. W. Woolerton, S. Sheard, Y. S. Chaudhary, F. A. Armstrong, *Energy & Environmental Science* **2012**, *5*, 7470-7490; c) F. Schwizer, Y. Okamoto, T. Heinisch, Y. Gu, M. M. Pellizzoni, V. Lebrun, R. Reuter, V. Köhler, J. C. Lewis, T. R. Ward, *Chemical Reviews* **2018**, *118*, 142-231.

[26] L. E. Roth, J. C. Nguyen, F. A. Tezcan, *Journal of the American Chemical Society* **2010**, *132*, 13672-13674.

[27] a) S. R. Soltau, J. Niklas, P. D. Dahlberg, O. G. Poluektov, D. M. Tiede, K. L. Mulfort, L. M. Utschig, *Chemical Communications* **2015**, *51*, 10628-10631; b) S. R. Soltau, P. D. Dahlberg, J. Niklas, O. G. Poluektov, K. L. Mulfort, L. M. Utschig, *Chemical Science* **2016**, *7*, 7068-7078; c) S. R. Soltau, J. Niklas, P. D. Dahlberg, K. L. Mulfort, O. G. Poluektov, L. M. Utschig, *ACS Energy Letters* **2017**, *2*, 230-237.

[28] M. Breuer, K. M. Rosso, J. Blumberger, *Proceedings of the National Academy of Sciences of the United States of America* **2014**, *111*, 611-616.

[29] a) P. Cedervall, A. B. Hooper, C. M. Wilmot, *Biochemistry* **2013**, *52*, 6211-6218; b) M. Czjzek, L. ElAntak, V. Zamboni, X. Morelli, A. Dolla, F. Guerlesquin, M. Bruschi, *Structure* **2002**, *10*, 1677-1686; c) M. J. Edwards, G. F. White, M. Norman, A. Tome-Fernandez, E. Ainsworth, L. Shi, J. K. Fredrickson, J. M. Zachara, J. N. Butt, D. J. Richardson, T. A. Clarke, **2015**; d) T. A. Clarke, M. J. Edwards, A. J. Gates, A. Hall, G. F. White, J. Bradley, C. L. Reardon, L. Shi, A. S. Beliaev, M. J. Marshall, Z. Wang, N. J. Watmough, J. K. Fredrickson, J. M. Zachara, J. N. Butt, D. J. Richardson, *Proceedings of the National Academy of Sciences of the United States of America* **2011**, *108*, 9384-9389; e) B. Hermann, M. Kern, L. La Pietra, J. Simon, O. Einsle, *Nature* **2015**, *520*, 706.

[30] L. Shi, S. M. Belchik, A. E. Plymale, S. Heald, A. C. Dohnalkova, K. Sybirna, H. Bottin, T. C. Squier, J. M. Zachara, J. K. Fredrickson, *Applied and environmental microbiology* **2011**, *77*, 5584-5590.

[31] T. G. Schmidt, L. Batz, L. Bonet, U. Carl, G. Holzapfel, K. Kiem, K. Matulewicz, D. Niermeier, I. Schuchardt, K. Stanar, *Protein expression and purification* **2013**, *92*, 54-61.

[32] T. Peters, in *Advances in Protein Chemistry, Vol. 37* (Eds.: C. B. Anfinsen, J. T. Edsall, F. M. Richards), Academic Press, **1985**, pp. 161-245.

[33] L. J. Anderson, D. J. Richardson, J. N. Butt, *Biochemistry* **2001**, *40*, 11294-11307.

10.1002/cbic.201800313

WILEY-VCH

Entry for the Table of Contents

FULL PAPER

Biohybrid phototransducers of visible light to electricity. We produced tetraheme cytochromes photosensitised by attachment of a Ru(II) dye. The site of Ru(II)-labelling defined whether the resulting bihybrids acted as molecular wires or resistors when irradiated in the presence of a sacrificial electron donor.

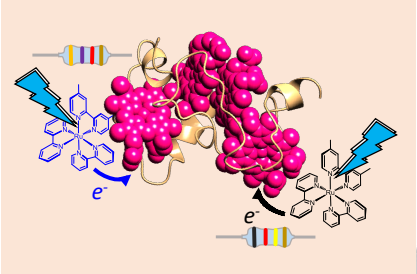

*Jessica H. van Wonderen, Daobo Li, Samuel E. H. Piper, Cheuk Y. Lau, Leon P. Jenner, Christopher R. Hall, Thomas A. Clarke, Nicholas J. Watmough and Julea N. Butt**

Page No. – Page No.
Photosensitised multi-heme cytochromes as light-driven molecular wires and resistors